Chemistry & Biology
Article

Substrate-Guided Design of a Potent and Selective Kallikrein-Related Peptidase Inhibitor for Kallikrein 4

Joakim E. Swedberg,[1] Laura V. Nigon,[1] Janet C. Reid,[1] Simon J. de Veer,[1] Carina M. Walpole,[1] Carson R. Stephens,[1] Terry P. Walsh,[1] Thomas K. Takayama,[2] John D. Hooper,[1] Judith A. Clements,[1] Ashley M. Buckle,[3] and Jonathan M. Harris[1,*]

[1]Institute of Health and Biomedical Innovation, Queensland University of Technology, Brisbane, Queensland 4059, Australia
[2]Departments of Biochemistry and Urology, University of Washington, Box 357350, Seattle, WA 98195-7350, USA
[3]Department of Biochemistry and Molecular Biology, School of Biomedical Sciences, Faculty of Medicine and Victorian Bioinformatics Consortium, Monash University, Clayton, Victoria 3800, Australia
*Correspondence: j2.harris@qut.edu.au
DOI 10.1016/j.chembiol.2009.05.008

SUMMARY

Human kallikrein-related peptidase 4 (KLK4/prostase), a trypsin-like serine protease, is a potential target for prostate cancer treatment because of its proteolytic ability to activate many tumorigenic and metastatic pathways including the protease activated receptors (PARs). Currently there are no KLK4-specific small-molecule inhibitors available for therapeutic development. Here we re-engineer the naturally occurring sunflower trypsin inhibitor to selectively block the proteolytic activity of KLK4 and prevent stimulation of PAR activity in a cell-based system. The re-engineered inhibitor was designed using a combination of molecular modeling and sparse matrix substrate screening.

INTRODUCTION

Prostate cancer is responsible for 10% of all male cancer deaths in the United States (Jemal et al., 2008) and is the most common newly diagnosed cancer in men. Current treatments for prostate cancer focus on androgen deprivation and are associated with a plethora of side effects (Malone et al., 2005) with no effective treatment available for late stages of the disease. Kallikrein-related peptidase 4 (KLK4) is a member of the tissue kallikrein family of serine proteases. It is predominantly expressed in basal and secretory cells of the prostate gland and is overexpressed in malignant prostate tumors (Veveris-Lowe et al., 2005; Xi et al., 2004). A series of in vitro studies have shown that KLK4 possesses proteolytic activities that are strongly linked to the development and progression of cancer. For example, KLK4 cleaves fibrinogen (Obiezu et al., 2006), a basic constituent of the extracellular matrix and an important factor in metastasis (Coughlin, 1999). Other relevant proteins targeted by KLK4 include collagen I and IV (Obiezu et al., 2006), prostatic acid phosphatase (Takayama et al., 1997), insulin-like growth factor binding protein (Matsumura et al., 2005), and urokinase plasminogen activator receptor (uPAR) (Beaufort et al., 2006).

Very recent studies have shown that KLK4 is also able to stimulate the activity of the protease activated receptors, PAR-1 and PAR-2 (Mize et al., 2008; Ramsay et al., 2008b), causing increased cell migration and proliferation. The PARs are a subfamily of the G-protein-coupled receptors that do not bind a soluble ligand, but instead are activated by specific proteolytic cleavage at their amino termini. This cleavage creates a new amino terminus that acts as a tethered ligand enabling receptor signaling (Coughlin, 2005; Hollenberg, 2003). Recently it was found that PAR-1 and PAR-2 were overexpressed in prostate cancer and that PAR-1- and PAR-2-specific agonists caused RhoA-dependent cytoskeletal remodelling (Mize et al., 2008). Furthermore, a number of other cancers show PAR-driven growth (Darmoul et al., 2001), invasion (Even-Ram et al., 1998; Henrikson et al., 1999), and metastasis (Nierodzik et al., 1998).

Of note, KLK4 is associated with an epithelial to mesenchymal transition-like effect and increased in vitro cell migration rates (Veveris-Lowe et al., 2005), which might reflect a PAR-induced event. KLK4 is also highly expressed in bone metastasis and thus might be involved in metastatic spread to bone tissue (Gao et al., 2007). These observations suggest KLK4 plays an important role in prostate cancer. However, there are currently no KLK4-specific small-molecule inhibitors, nor are there specific inhibitors available for the other 15 members of the kallikrein-related peptidase group of enzymes to which KLK4 belongs. This lack might reflect the difficulty associated with selective inhibition of an individual member of a closely related superfamily of enzymes. Indeed, the kallikreins share very high homology when considering the surface of their active sites, with KLK14 and KLK4 showing 85% amino acid identity within 5 Å of their catalytic triads. Despite the lack of synthetic inhibitors, there are a number of naturally occurring molecules that can block serine protease activity including sunflower trypsin inhibitor (SFTI or SFTI-1).

SFTI belongs to the Bowman-Birk serine protease inhibitor family and is a potent inhibitor of trypsin and cathepsin G, and a suppressor of tumorigenesis 14 (ST14/matriptase/MT-SP1). It was recently discovered in sunflower (*Helianthus annus*) seeds and characterized by determination of its three-dimensional structure in complex with bovine β-trypsin (Luckett et al., 1999). Trypsin exhibits a high level of sequence homology to

the kallikrein-related protease KLK4 (73% homology within 6 Å of the catalytic triad), suggesting that SFTI might also inhibit this enzyme. Despite SFTI's considerable potential as a generic protease inhibitor, to date there have been no systematic attempts to engineer the molecule to produce a potent ***and*** highly selective protease inhibitor.

This study focuses on production of a potent and selective KLK inhibitor by substrate guided design methods. KLK4 was chosen to initiate this study because its peptide substrate specificity has recently been investigated in two studies using positional scanning synthetic combinatorial libraries (PS-SCL) of tetrapeptides (Debela et al., 2006; Matsumura et al., 2005). In both studies, individual peptide substrates representative of optimal sequences were not assayed. Furthermore, there were disparities between the two studies regarding ranking of cleavage sites for KLK4, suggesting that the optimal KLK4 cleavage specificity is yet to be defined. Accordingly, we set out to design a sparse matrix peptide library of 125 individual tetrapeptide-*para*-nitroanilides (*p*NAs) representing all possible combinations in position P2, P3, and P4 of the five highest scoring residues in the previous study of Matsumura and co-workers (Matsumura et al., 2005). In contrast to this previous study, we chose to synthesize our library in serial mode (individually) rather than through a multiplexed (mixed) PS-SCL scheme. Once found, the optimal cleavage sequence formed the basis for re-engineering of SFTI and production of a potent inhibitor that could provide a novel treatment for KLK4-driven effects in prostate cancer.

RESULTS

Rational Design of a Small-Molecule KLK4 Inhibitor

Our design strategy consisted of three discrete steps. Initially we screened a focused tetrapeptide library of *p*NA substrates to determine the optimal substrate for KLK4, which revealed that the sequence FVQR outperformed previous candidate substrates. We then used this sequence to design an intermediate peptide aldehyde inhibitor to verify our hypothesis that efficient substrates for KLK4 could also be used as the basis of efficient inhibitors, and finally substituted the optimal tetrapeptide sequence into the SFTI scaffold to produce an inhibitor with an amidolytic K_i of 3.59 ± 0.28 nM.

KLK4 Has a Marked Preference for a Phenyl Group at P4 and FVQR Is its Optimal Tetrapeptide Substrate

Enhancement of the potency and selectivity of inhibition of the wild-type SFTI toward KLK4 required a detailed knowledge of the enzyme's ligand-binding determinants. Accordingly, we probed the enzyme active site with a sparse matrix library of chromogenic peptide substrates. Results from the library screen are summarized in Figure 1. The substrate FVQR-*p*NA was hydrolyzed most efficiently (6.7 times average rate) followed by FTQR-*p*NA and IVQR-*p*NA (4.4 and 4.3 times average rates, respectively). Significantly, IVQR had previously been predicted to be the optimal tetrapeptide substrate for KLK4 (Debela et al., 2006).

KLK4 has previously been shown to have highest amidolytic activity toward the standard tripeptide substrate Bz-FVR-*p*NA out of all experimentally tested colorimetric peptide substrates (Matsumura et al., 2005). Therefore, we decided to use this substrate as a benchmark when determining KLK4's enzymatic activity toward FVQR-*p*NA. A number of peptide *p*NA substrates were synthesized, purified, and further characterized. Given the preference for phenyl and bulky hydrophobic residues at the N terminus of the peptide substrates as determined in these studies, we examined the contribution of the benzoyl capping group of Bz-FVR-*p*NA to its apparent preference as an amidolytic substrate for KLK4. Accordingly, we evaluated an acetylated variant, Ac-FVR-*p*NA, and because IVQR scored second best in the sparse matrix library and had previously been suggested to be the optimal KLK4 cleavage sequence (Debela et al., 2006), IVQR-*p*NA was also included. In addition, we also synthesized FVMR-*p*NA to assess the importance of the preference we observed for the polar glutamine residue in the P2 position by replacing it with a more hydrophobic methionine residue. Kinetic data for these substrates are summarized in Table 1. KLK4 showed highest amidolytic activity toward FVQR-*p*NA of all chromogenic substrates examined. Replacing the N-terminal benzoyl group of Bz-FVR-*p*NA with an acetyl group resulted in a 47% reduction of k_{cat} whereas replacing Phe with Val at the P4 position resulted in an 87% reduction of k_{cat}, indicating an important role of the benzene ring in the interaction with KLK4 at the P4 position. The considerable reduction in k_{cat} as a result of replacing Gln with Met in the S2 or P2 position suggests that the polarity of the Gln side chain plays an important role in the rate of hydrolysis of this substrate. As a result of this, we used the sequence FVQR as the basis of inhibitor design rather than IVQR and FQQR, as predicted previously (Matsumura et al., 2005; Debela et al., 2006), or the commercially available tripeptide benzoyl FVR-*p*NA that until now has been considered the substrate with highest k_{cat}.

Peptide Aldehydes Based on Substrate Sequences Are Inhibitors of KLK4

We hypothesized that sequences that were efficient substrates for KLK4 would be complementary to the S1–S4 subsites of the enzyme's catalytic center. Consequently, we created a series of peptide aldehydes based on the optimal sequence from our sparse matrix peptide library, the best substrate predicted by PS-SCL (IVQR) and an aldehyde based on Bz-FVR-*p*NA. The aldehyde groups on these compounds mimic the transition state of the amidolytic reaction, producing molecules that inhibit proteolysis. The two library-based aldehydes inhibited KLK4 amidolytic activity at micromolar levels, whereas Bz-FVR aldehyde did not inhibit KLK4 in this range (data not shown). FVQR aldehyde was the most efficient inhibitor by an order of magnitude with an IC_{50} of 10.8 ± 1.3 μM compared with 103.3 ± 2.8 μM for IVQR. Although these levels of inhibition are not therapeutically useful, they serve to validate our approach.

KLK4 Is Inhibited by Wild-Type SFTI

Given that trypsin and KLK4 share significant structural (root-mean-square deviation [rmsd] = 1.1 Å over 223 Cα atoms) and sequence similarity (40% overall and 73% identity within the area adjacent to SFTI in the crystal structure, PDB ID 1SFI) and are both trypsin-like serine proteases, we reasoned that SFTI would be able to inhibit KLK4 in addition to trypsin. Assays with the amidolytic standard KLK4 substrate Bz-FVR-*p*NA showed that the wild-type inhibitor could indeed block KLK4 activity with an IC_{50} of 221.4 ± 1.1 nM.

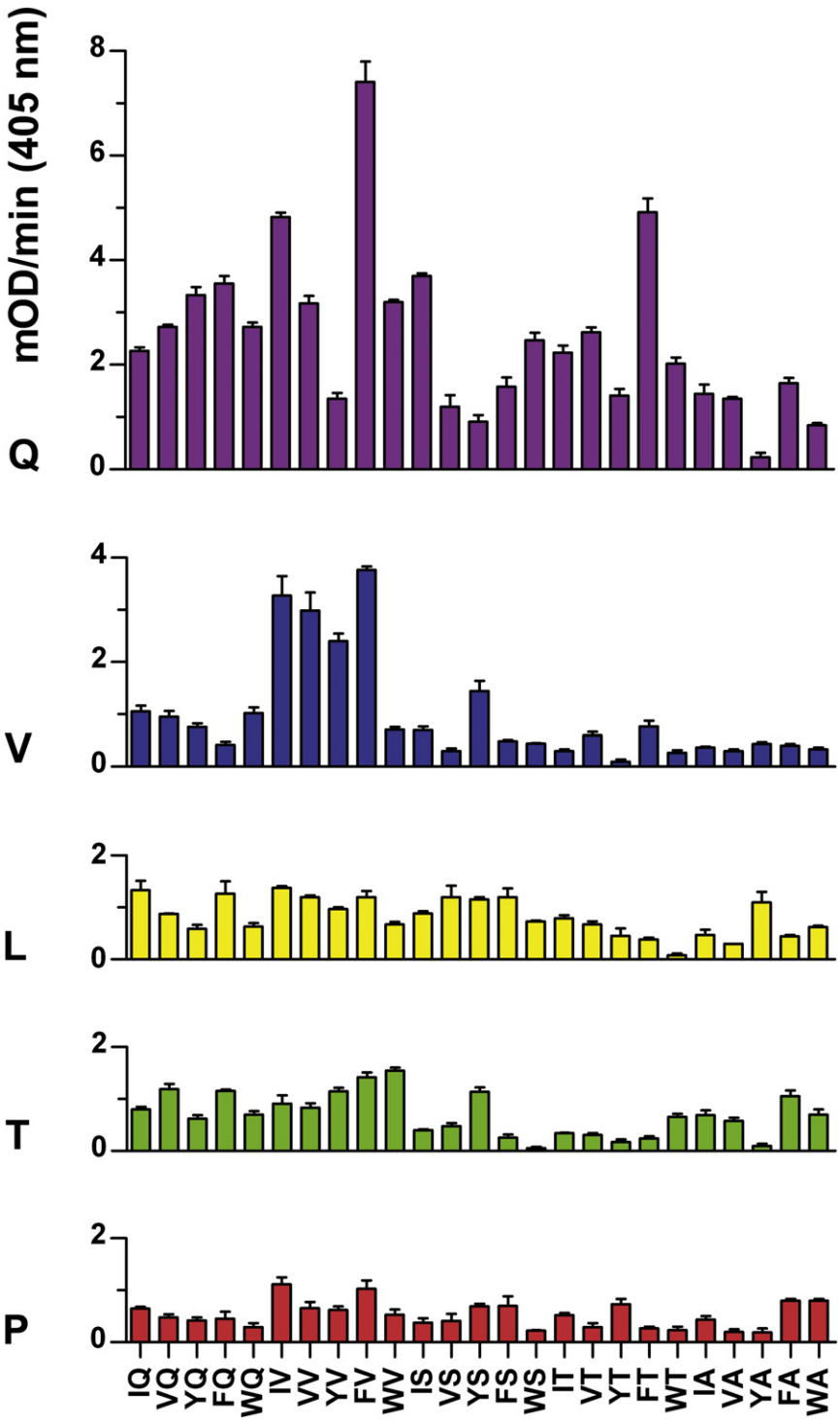

Figure 1. Amidolytic Activity of KLK4 against Sparse Matrix Library *p*NA Substrates

The *y* axis represents the rate of substrate cleavage in mOD/min(405), with the amino acid at position P2 indicated beside each *y* axis. The *x* axis labels the bars corresponding to substrates with each of the 25 combinations of the amino acids in the P4 and P3 positions. Arginine was kept constant in the P1 position while varying the amino acid in positions P2–P4 as indicated in the graph. Data represent mean and standard error of the mean (± SEM) of three experiments in triplicate.

SFTI-FCQR Is a Potent Selective Inhibitor of KLK4

KLK4 showed a marked preference for the sequence FVQR as a substrate for cleavage and as an aldehyde inhibitor. Accordingly, we decided to substitute this sequence into the SFTI backbone to increase the scaffold's potency of inhibition. The variant SFTI molecule was designed such that the key P1 residue (Lys5) was replaced by arginine, with glutamine replacing Thr4. Cys3 was not substituted given the pivotal role of this residue in the structural stability of SFTI, while Arg2 was replaced by phenylalanine. Inhibitory potency of the resulting variant (SFTI-FCQR) was evaluated against KLK4. Enzyme velocities were monitored with varying inhibitor concentration in the range of 2.0 μM to 1 nM to determine IC_{50} (Bz-FVR-*p*NA; 0.12 mM) and K_i (FVQR-*p*NA) values. SFTI-FCQR was determined to be a potent KLK4 inhibitor with an IC_{50} of 7.97 ± 1.08 nM and a K_i of 3.59 ± 0.28 nM (Table 2).

Wild-type SFTI displays promiscuous inhibition, blocking the activity of diverse proteases including suppressor of tumorigenesis 14 (ST14/matriptase) and cathepsin G in addition to trypsin. Accordingly, we assayed a panel of serine proteases including trypsin, thrombin, α-chymotrypsin, *Streptomyces griseus* type XIV protease, plasminogen protease, and suppressor of tumorigenesis 14 ST14/matriptase to assess their inhibition by SFTI-FCQR. We found that the SFTI variant did not inhibit any of these proteases, with the exception of trypsin, which was only inhibited in the micromolar range (IC_{50} 4.064 ± 1.088 μM; Table 2). As a further test of the inhibitor's selectivity we also tested the closely related trypsin-like serine proteases of the kallikrein related peptidase superfamily, namely KLK2, 5 and 14. KLK14 in particular shares 85% amino acid identity with KLK4 within 5 Å of the active site catalytic triad and yet SFTI-FCQR only inhibited the enzyme at micromolar levels (see Table 2).

While inhibition of serine proteases is most usually measured using small peptide and ester substrates, the important biological activities of the enzymes are the result of protein proteolysis. Given this, we also assayed both the wild-type and FCQR variant inhibitors for their ability to inhibit KLK4 proteolysis of fibrinogen,

Table 1. K_M, k_{cat} and Catalytic Efficiency (k_{cat}/K_M) for *para*-Nitroanilide Substrates

Substrate	K_M	k_{cat}	k_{cat}/K_M
Bz-FVR-*p*NA	42.5 ± 5.9 μM	1.89 ± 0.10 s^{-1}	41.54 ± 4.65 × 10^3 M^{-1} s^{-1}
Ac-FVR-*p*NA	194.9 ± 41.4 μM	1.00 ± 0.11 s^{-1}	1.00 ± 0.11 × 10^3 M^{-1} s^{-1}
FVMR-*p*NA	74.7 ± 10.3 μM	1.27 ± 0.063 s^{-1}	17.00 ± 0.50 × 10^3 M^{-1} s^{-1}
IVQR-*p*NA	183.1 ± 12.14 μM	2.10 ± 0.23 s^{-1}	11.47 ± 0.23 × 10^3 M^{-1} s^{-1}
FVQR-*p*NA	679.9 ± 113.1 μM	15.7 ± 1.57 s^{-1}	23.09 ± 0.63 × 10^3 M^{-1} s^{-1}

a known substrate for the enzyme (Obiezu et al., 2006). Surprisingly, inhibition of fibrinogen proteolysis did not reflect inhibition of peptide-*p*NA hydrolysis. The FCQR variant was found to be a potent inhibitor of fibrinogen proteolysis by KLK4, with complete inhibition at 250 nM (Figure 2A). Unexpectedly, no inhibition of proteolysis by KLK4 could be detected for the wild-type inhibitor even at a concentration of 2 μM, compared to a substrate concentration of 0.8 μM and an enzyme concentration of 2.5 nM (Figure 2A), a marked contrast to the inhibition of amidolytic activity. Similarly, the SFTI-FCQR variant showed no inhibition of tryptic digestion of fibrinogen up to a concentration of 2 μM (Figure 2B), or with KLK2, 5, 12, and 14 (see Figures 2C–2F).

SFTI-FCQR Maintains its Inhibitory Activity with a Half-Life of 4 Days in Tissue Culture

To gauge the half-life of SFTI-FCQR in a cellular environment, we incubated STFI-FCQR at a concentration of 1 μM with LNCaP, 22Rv1, and PC3 prostate cancer cell lines. Residual SFTI-FCQR inhibitory activity was measured in tissue culture supernatants that had been boiled and centrifuged to remove serum derived protease inhibitors. Assaying a 1:5 dilution of tissue culture supernatant (200 nM concentration at time = 0) against recombinant KLK4 gave complete inhibition even after a week of contact with prostate cancer cells (data not shown). Dilution by a further 20-fold was required before any appreciable reduction of inhibitory activity could be observed. Half-lives for inhibitor incubated with LNCaP and 22Rv1 were similar (Figure 3; $t_{1/2}$ = 119 hr and 117 hr, respectively), whereas the decline in inhibition was accelerated in PC3s ($t_{1/2}$ = 89hr). Decay of inhibition followed a secondary polynomial relationship, with the exponential component being concurrent for all three cell lines, whereas the linear component was nearly five times greater in the presence of PC3s. This difference might correlate with the higher metabolic rate observed in this cell line compared with LNCaP and 22Rv1 as determined by WST-1 assays (data not shown). Although these half-life measurements do not allow estimation of in vivo clearance from circulation via the kidneys, they argue that SFTI-FCQR enjoys considerable stability in the cellular milieu.

SFTI-FCQR Blocks KLK4 Stimulated Calcium Flux in Cell-Based Assays

Recent work has demonstrated that KLK4 is able to stimulate the protease activated receptors PAR-1 and PAR-2, causing release of intracellular calcium, phosphorylation of ERK1/2, and ultimately increasing rates of proliferation in DU145 prostate cancer cells (Ramsay et al., 2008b; Mize et al., 2008). These effects could be blocked by the nonspecific protease inhibitor aprotinin.

Table 2. Inhibitory Properties of Wild-Type SFTI and SFTI-FCQR

Enzyme	Inhibitor	K_i (nM)	Substrate	IC_{50} (nM)	Substrate (0.1 mM)
KLK4	SFTI-1	—	—	221.4 ± 10.1	Bz-FVR-*p*NA
	SFTI-FCQR	3.59 ± 0.28	FVQR-*p*NA	7.97 ± 1.08	FVQR-*p*NA
KLK2	SFTI-FCQR	—	—	>10,000	Bz-PFR-*p*NA
KLK5	SFTI-FCQR	—	—	2348 ± 721	Bz-PFR-*p*NA
KLK14	SFTI-FCQR	—	—	1506 ± 37.1	Ac-GSLR-*p*NA
β-Trypsin	SFTI-1	0.1[a]	BAPNA	—	—
	SFTI-FCQR	—	—	4064 ± 1088	BAPNA
Thrombin	SFTI-1	136[a]	Unknown	—	—
		5050[b]	N-t-Boc-LRR-AMC	—	—
	SFTI-FCQR	—	—	>10,000	Bz-FVR-*p*NA
Matriptase	SFTI-1	0.92[b]	N-t-Boc-QAR-AMC	—	—
	SFTI-FCQR	—	—	>10,000	Bz-FVR-*p*NA
α-Chymotrypsin	SFTI-1	2300 ± 100[c]	N-succinyl-AAPP-*p*NA	1800 ± 110	W-*p*NA
	SFTI-FCQR	—	—	>10,000	W-*p*NA
Plasminogen	SFTI-FCQR	—	—	>10,000	L-*p*NA, BAPNA
Streptomyces griseus type XIV protease	SFTI-FCQR	—	—	>10,000	L-*p*NA, BAPNA

[a] Luckett et al., 1999
[b] Long et al., 2001
[c] Descours et al., 2002

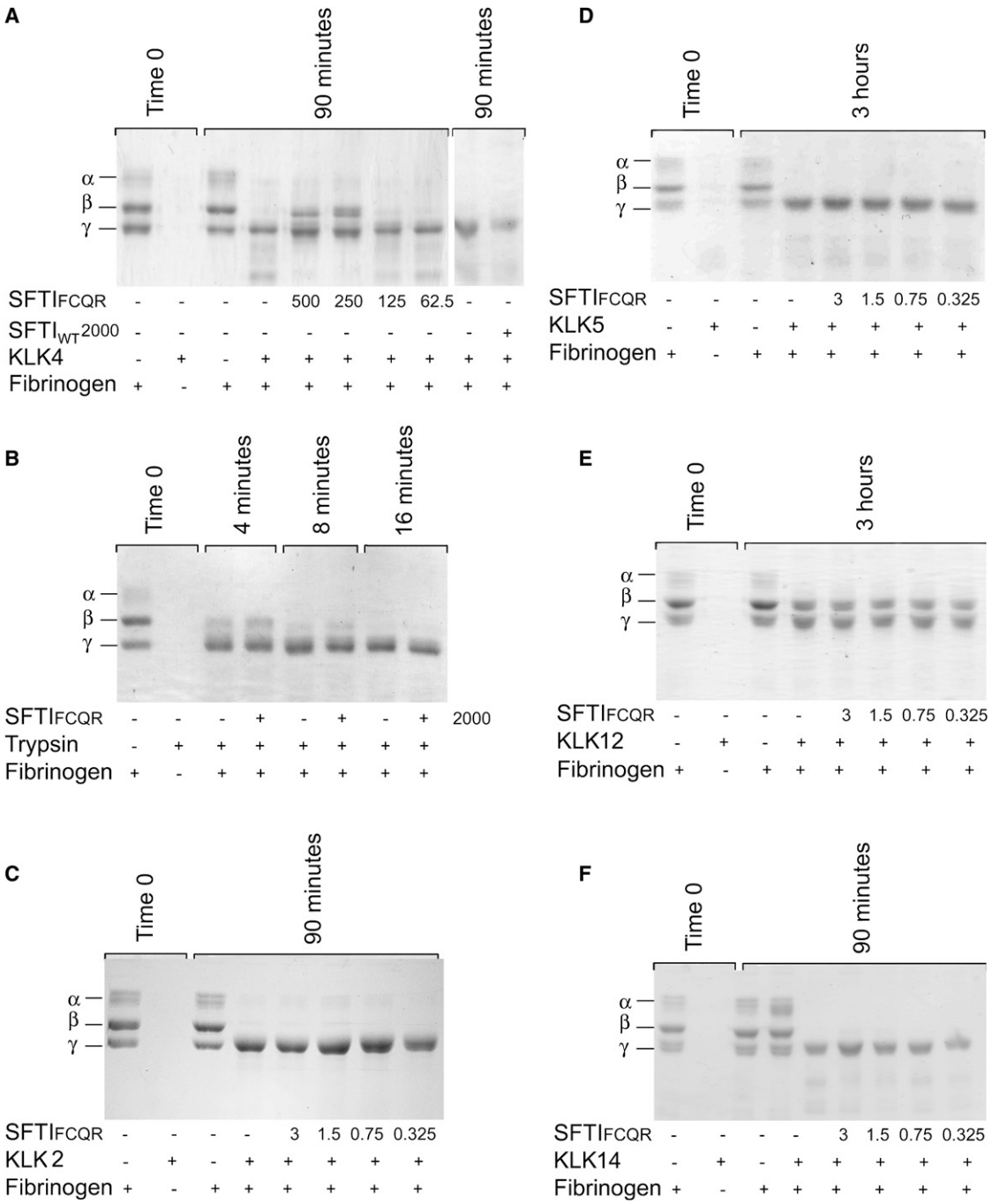

Figure 2. Inhibition of serine protease proteolytic activity by SFTI and SFTI-FCQR

Kallikrein and trypsin-mediated proteolysis of fibrinogen assessed by SDS-PAGE. Proteolytic products are visualized by Coomassie blue staining following resolution on 12% polyacrylamide gels.

(A) Effect of increasing concentrations of SFTI-FCQR on fibrinogen digestion by KLK4 and $SFTI_{wt}$ at a concentration of 2000 nM.

(B) Trypsin digestion of fibrinogen in the presence and absence of 2000 nM SFTI-FCQR.

(C–F) Digestion of fibrinogen by KLK2, 5, 12, and 14, respectively, in the presence of increasing concentrations of SFTI-FCQR. Gels are representative of three independent experiments.

We reasoned that SFTI-FCQR should also be able to block this activity, and assessed the inhibitor's effect on KLK4 stimulated calcium release in cell-based assays. The inhibitor showed extremely robust blockade of calcium release when stimulated by KLK4 treatment in the presence of 1 μM SFTI-FCQR (Figure 4). Furthermore, the inhibitor was selective, blocking KLK4 only and being permissive for calcium release by both trypsin and PAR-2-activating peptide.

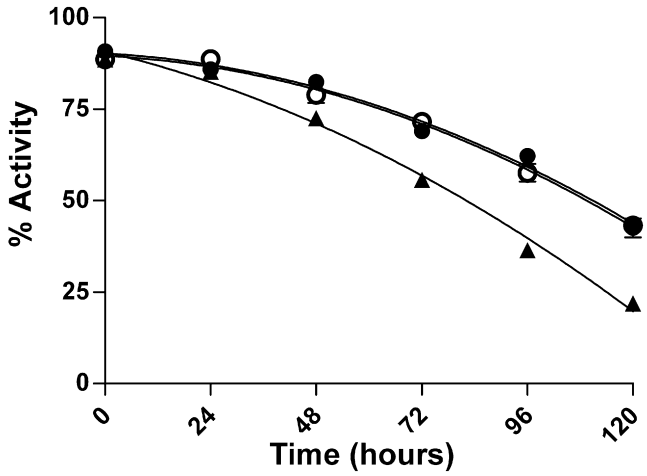

Figure 3. Stability of SFTI-FCQR in Contact with Prostate Cancer Cells In Vitro

Residual SFTI-FCQR was assayed in cell culture media from prostate cancer cells treated with a single 1 μM dose of inhibitor at time 0. Endogenous inhibitors were removed by boiling followed by centrifugation to remove precipitated denatured protein. Stability was assessed against LNCaP (closed circles), 22RV1 (open circles), and PC3 cells (triangles). Data are mean ± SEM from three experiments in triplicate.

Modeling a KLK4-SFTI-FCQR Complex

To gain a molecular understanding of the behavior of the substituted SFTI variant, we carried out predictive modeling of an SFTI-FCQR/KLK4 complex using the SFTI/trypsin structure 1SFI and the KLK4 structure 2BDG as starting point. Trypsin and KLK4 superimpose closely, with an RMSD of 1.1 Å over 223 Cα atoms. Active site regions superimpose extremely well, with the exception of residues that form the S4 subsite: residues 95–98 (the ''99 loop'') fold back, away from the active site of KLK4 in comparison with trypsin (Figure 5A), resulting in differences of up to 3 Å; residues in the 164–180 loop also display large differences. These differences have two important consequences. First, the side chains of L98, L99, and L175 in KLK4 move toward the S4 pocket, making it more hydrophobic. Second, the negative S2 pocket, with D102 (catalytic) at its base, widens and deepens, making it accessible by the substituted Gln in the SFTI-FCQR variant, which can H-bond with residues lining the pocket (Figures 5D and 5E).

Structural similarities between KLK4 and trypsin were reflected in the predicted structure for the SFTI-FCQR variant. The variant SFTI was modeled by simple substitution of the wild-type structure coupled with rotamer-based side-chain modeling and energy minimization. This produced only subtle atomic shifts that relieved close atomic contacts. Each substitution and subsequent structural changes in the context of KLK4-trypsin structural differences is discussed below. Particular attention is drawn to the net balance of hydrogen bonds and nonpolar interactions at the site of substitution.

K5R (P_1): The most statistically preferred Arg rotamer correlates well with the wild-type Lys side-chain conformation. Energy minimization relieves a close contact of K5 with S190 in the trypsin-SFTI complex and the modeled SFTI R5 side chain forms two hydrogen bonds with D189 at the base of the electronegative S1 pocket (Figures 5B and 5D). However, an intramolecular hydrogen bond with S10 is lost.

T4Q (P_2): Substitution of the Thr side chain in SFTI removes two intramolecular hydrogen bonds, with S6 and I10 of SFTI (Figure 5B). However, T4 does not hydrogen-bond with the protease. Modeling a Gln at this position (using the second most statistically preferred rotamer) in the SFTI-FCQR allows two hydrogen bonds between its side-chain amide group and the protease (catalytic H57 side chain and S214 main chain; Figure 5C). In addition, when adopting this conformation, the relatively larger side chain of Gln fits snugly into the S2 pocket that is wider in KLK4 compared with trypsin (Figures 5D and 5E).

R2F (P_4): The side chain of R2 in SFTI forms a hydrogen bond with the backbone of N97 of trypsin. A Phe at this position in SFTI-FCQR can be modeled satisfactorily using the most preferred rotamer, and makes nonpolar interactions with the side chains of L175 and F215 of the protease. In response to substitution, small movements of the side chain of D14 of the inhibitor (in order to remove unfavorable close contacts) result in the loss of a hydrogen bond between D14 and the SFTI backbone.

The preferences for residues at P1, P2, and P4 can be explained largely by the physicochemical nature of each subsite in the modeled complex, with the exception of the poor preference for Tyr at P4, compared with Phe. Indeed, in the current

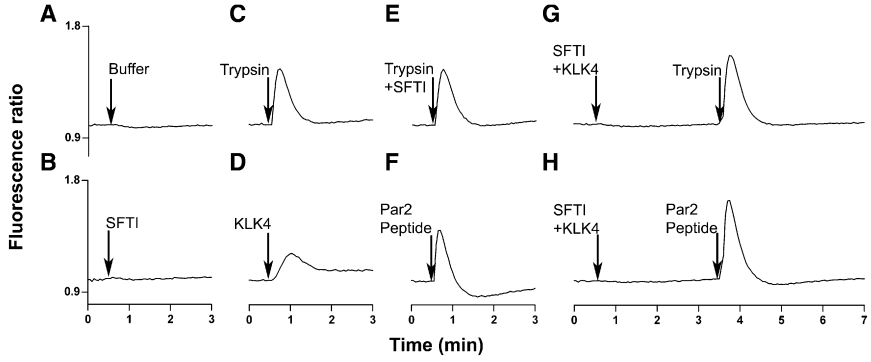

Figure 4. Effect of SFTI-FCQR on Calcium Release in Cell-Based Assays

Lung murine fibroblasts (LMF) stably expressing human PAR-2 were incubated after 30 s with either activated insect cell-derived KLK4 (iKLK4, 300 nM), trypsin (10 nM), or PAR-2-activating peptide (100 nM) with or without SFTI-FCQR (1 μM). The fluorescence at 510 nm was measured following alternating excitation at 340 and 380 nm (Em510[340/380]). The ratio of Em510(340/380) is proportional to intracellular Ca^{2+} ion concentration. The data are represented as mean of three experiments in triplicate. Treatment with (A) buffer or (B) SFTI-FCQR only had no effect whereas treatment with (C) trypsin, (D) iKLK4, (E) trypsin and SFTI-FCQR, or (F) PAR-2-activating peptide resulted in increased intracellular Ca^{2+} ion concentration. Calcium flux was restored in cells initially treated with iKLK4 and SFTI-FCQR at 30 s by addition of (G) trypsin or (H) PAR-2-activating peptide after 3.5 min. Arrows indicate injection points for solutions as indicated.

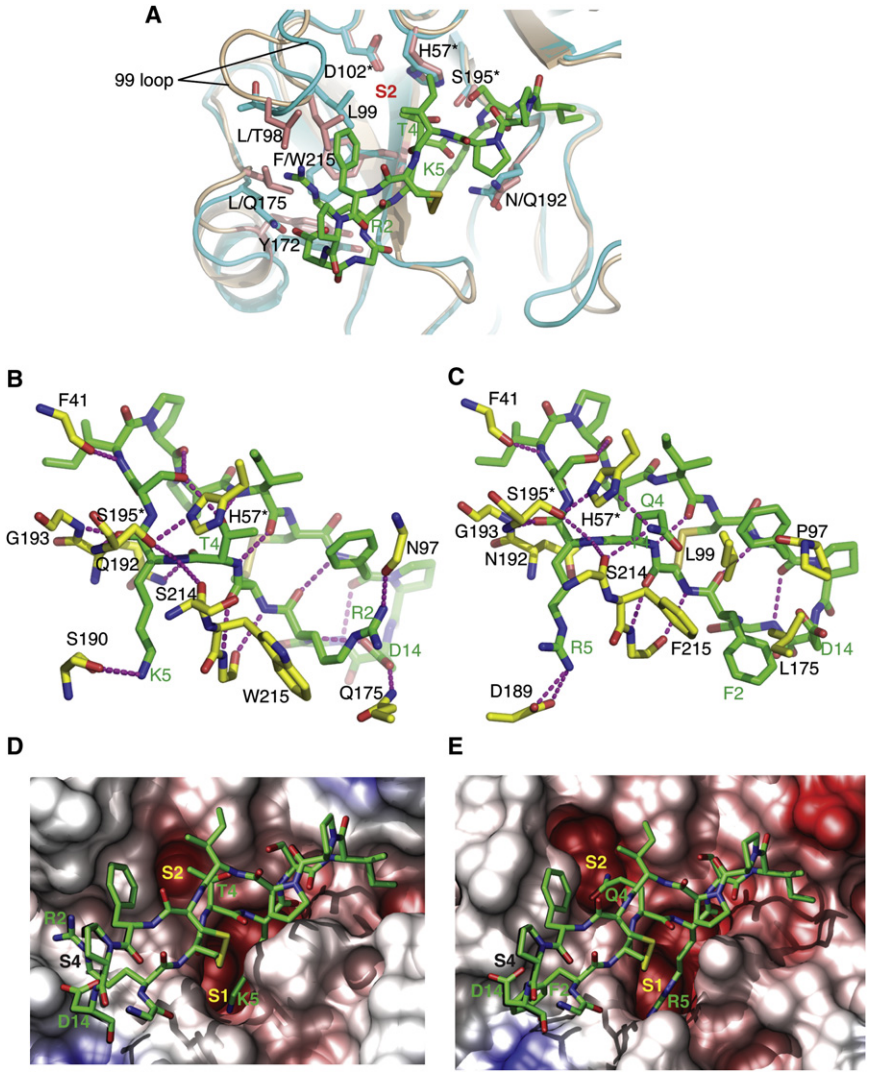

Figure 5. Structural Characteristics of the Protease-Inhibitor Interfaces for the Trypsin-SFTI and the Modeled KLK4/SFTI-FCQR Complex

Catalytic residues are labeled with an asterisk. SFTI residues that have been substituted in this study are labeled in green.

(A) Superposition between trypsin (cyan)-SFTI (green) complex (1SFI) and KLK4 (1BD1, pink) in and around the active site, showing regions of structural differences, notably around the "99 loop" (L/T98; L99) and at residue 175. Side chains are shown and labeled for sequence differences or where significant structural differences are observed (KLK residue shown before trypsin residue in label). The S2 subsite is indicated.

(B and C) Hydrogen bonds (magenta dashed lines) between trypsin (yellow) and SFTI (green) (B), and (C) modeled KLK4 (yellow) and SFTI-FCQR (green). Viewed from the inverse angle compared with all other figures in panel, i.e., view from protease toward inhibitor.

(D and E) Molecular surfaces of (D) trypsin-SFTI and (E) modeled KLK4-SFTI-FCQR complexes colored according to electrostatic potential (red indicates negative, blue is positive). Subsites are labeled as S1, S2, etc. Structural differences between trypsin and KLK4, notably at L95 and L/T98, shown in A, cause an increase in the width and depth of the electronegative S2 pocket, allowing its occupation by the modeled glutamine (4Q) side chain of SFTI-FCQR.

model a tyrosine could be positioned in a similar orientation to the Phe, with neighboring polar groups positioned to form hydrogen bonds with its OH moiety. The poor preference for Tyr could be explained by assuming an alternative side-chain rotamer that positions its side chain deeper into the hydrophobic core created by residues L99, L175, and F215 (data not shown). The absence of polar hydrogen-bonding partners for the OH moiety would destabilize this residue, rationalizing the experimental data presented here. However, modeling Tyr at this position produces several close contacts with neighboring residues that can only be relieved by relatively large structural rearrangements in the surroundings. These cannot be modeled with any accuracy using current molecular simulation techniques, and therefore a full structural rationalization must await high-resolution crystallographic analysis.

DISCUSSION

This study has used substrate-based and computer-aided design to develop a highly selective protease inhibitor that can block signaling by protease-activated receptors in a cellular context. Specifically, we have shown that a peptide sequence that performs well as a substrate for a target protease can be substituted into the naturally occurring SFTI scaffold to produce an inhibitor with a nanomolar K_i. The inhibitor displayed reduced ability to inhibit the proteases thrombin and suppressor of tumorigenesis 14 (ST14/matriptase) by three orders of magnitude and achieved differential inhibition of trypsin-like proteases from the kallikrein related peptidase superfamily. We have also demonstrated that inhibition of peptide cleavage by a protease does not necessarily reflect inhibition of cleavage of protein substrates, an important caveat for screening potential lead compounds directed at proteases. Furthermore, this study illustrates the extreme robustness of the SFTI scaffold toward degradation in a cellular context refuting previous studies which focused on engineering the supposedly labile disulphide bond.

Previously we have shown that PAR-1 and PAR-2 are upregulated in prostate cancer cells (Ramsay et al., 2008b) and that PAR-1 and PAR-2 activity plays a role in proliferation and migration of prostate cancer cells (Mize et al., 2008). Accordingly, PAR activity is an attractive target for chemotherapeutic intervention. Here we have inhibited the stimulation of PAR-2 by its putative cognate in vivo protease, KLK4, which is also upregulated during prostate cancer progression. PAR-2 inhibition was assessed in cell-based assays, which demonstrated the potency of inhibition

by our SFTI variant by complete inhibition of calcium flux at a concentration of 1 μM. Significantly, the inhibitor had no effect on trypsin stimulated calcium flux or on PAR-2 activity elicited by an exogenously added PAR-2-activating peptide. The inhibitory activity of SFTI-FCQR could form the basis of a novel treatment for prostate cancer. This prospect has been enhanced by our finding that the variant inhibitor is highly robust with a half-life measured in days in tissue culture conditions, even when considering PC3 cells with very high metabolic activity.

The SFTI scaffold represents an excellent platform for drug design. With only 14 amino acids and a molecular mass of 1.513 kDa, SFTI is one of the smallest naturally occurring serine protease inhibitors (Luckett et al., 1999) having very high potency of inhibition (β-trypsin: K_i = 0.1nM). Comparison of the structure of SFTI in complex with β-trypsin and in solution (Korsinczky et al., 2001) indicates that the peptide's conformation does not change markedly upon binding to the protease, reflecting stabilization of the inhibitor both by cyclization and a bisecting disulphide bond. SFTI's disulphide bond is regarded as something of an Achilles' heel, with a potential for thiol-disulfide exchange reactions with reduced glutathione and other redox active species (Huck et al., 2006). This has led to a series of studies replacing the natural disulphide bond with a series of olefinic and other substituted linkers (Li et al., 2007). Although the results of these studies are interesting, a careful examination of the disulphide's flanking sequence would have shown that it is actually intrinsically resistant to exchange reactions. Important determinants of disulfide bond stability include neighboring residues of aromatic and amino side chains near the bond greatly reducing and increasing the reactivity, respectively (Huck et al., 2006; Snyder et al., 1981). The disulfide bond in SFTI-FCQR is surrounded by Phe2 and Gln4 on one side and Ile10 and Phe12 on the other side. Because Gln4 is extended as far as sterically possible away from the disulfide bond due to a hydrogen bond with Ser6, the disulfide bond is likely to be quite stable as revealed by its extended half-life in tissue-culture-based assays. The significant factor here is that maintaining the native disulphide bond preserves the option of biological manufacture through the sunflower seed system, which is not possible with the olefinic derivatives produced in the previous studies.

SFTI's constrained geometry and potency of inhibition have focused drug design efforts on the molecule's potential as a generic scaffold for protease inhibitor construction (Hilpert et al., 2005). An alanine scanning study of SFTI revealed little variation of the potency of inhibition after substitution of individual residues within the molecule, with the exception of the replacement of Lys5, which resulted in a 1000-fold decrease in inhibition of bovine trypsin (Daly et al., 2006). Several other studies used conservative substitution of amino acids around the SFTI ring to produce inhibitors that were active against bovine trypsin, chymotrypsin, and human elastase (Daly et al., 2006: Li et al., 2007; Zablotna et al., 2007). However, these studies did not examine the ability of their respective SFTI variants to inhibit proteolysis of full-length protein substrates, but relied on inhibition of activity toward standard amidolytic substrates. Additionally, they did not assess the selectivity of their inhibitors with closely related proteases. Use of SFTI as a molecular scaffold for designing potent and specific inhibitors is particularly challenging because of the molecule's broad selectivity of inhibition (K_i in the nanomolar range for the three unrelated proteases: ST14, trypsin, and cathepsin G [Long et al., 2001]).

In contrast to the reports above, the inhibitor resulting from these studies has both enhanced inhibitory potency ***and*** selectivity. The importance of inhibitor selectivity has been highlighted by recent failures in clinical trials of a series of metalloproteinase (MMP) inhibitors that were developed in an attempt to block MMP-mediated digestion of extracellular matrix components and halt tumor progression (Chambers and Matrisian, 1997). Some of these entered phase 3 clinical trials (Hidalgo and Eckhardt, 2001), although most have been terminated due to no or negative survival benefits (Overall and Lopez-Otin, 2002). It has been suggested that these negative outcomes reflect the lack of selectivity in these inhibitors, resulting in interference with other non-pathology-related physiological processes (Arlt et al., 2002; Kruger et al., 2001).

The role of selectivity and affinity is further attested to by the failure of the wild-type SFTI to inhibit digestion of fibrinogen by KLK4. Hence, although the wild-type SFTI might bind with high affinity to KLK4, it has lower selectivity than the FCQR variant we describe. This is especially important in view of the pivotal role that fibrinogen remodelling plays in maintenance of the extracellular matrix and progression of cancer. Furthermore, we propose that although wild-type SFTI might compete efficiently with a short peptide for the enzyme's active site, it is completely ineffective when competing with a larger protein binding with higher affinity and selectivity when compared with the FCQR variant, with its superior selectivity as attested to by its lack of inhibition of KLK2, 5, 12, and 14 proteolysis. The failure of the wild-type SFTI to inhibit protein proteolysis in the context of successful inhibition of hydrolysis of a peptide *p*NA also has important implications for the way in which the inhibition of protease activity is assessed. It is possible that this phenomenon is restricted to certain proteases and the *p*NA reporter group. However, if differential inhibition of peptide hydrolysis versus protein hydrolysis is more general, a large number of studies relying on inhibition of hydrolysis of model substrates might have been erroneously extended to cover inhibition of in vivo protein degradation.

SIGNIFICANCE

Recently PAR activity has become the focus of considerable attention because of its demonstrated role in cellular proliferation and migration in cancer cell lines, in addition to the discovery that it is overexpressed during prostate cancer progression. Here we have actively targeted the proteolytic activation of PAR-2 by the serine protease KLK4 on the basis of the temporal coexpression of these proteins (Ramsay et al., 2008a). Our work has resulted in the first serine protease inhibitor to selectively and potently inhibit KLK4 activation of PAR-2. One of the main challenges in protease inhibitor design has been the ability to produce molecules that potently inhibit target proteases but that leave other important proteolytic processes unaffected. Although we have not assayed all other serine proteases, we have demonstrated the selectivity of our SFTI variant against KLK4's closest relatives. In contrast to conventional strategies, we have used a library composed of individual peptides

to produce an aldehyde-based inhibitor with an IC_{50} an order of magnitude lower than that selected from a previously published positional scanning library. We then used the novel strategy of substituting this sequence into the naturally occurring SFTI scaffold that is already a highly potent inhibitor of serine proteases, but lacks selectivity. Our design strategy resulted in an inhibitor with a highly restricted range of inhibitory activity but retained its potency, achieving an IC_{50} value within an order of magnitude to that of the native inhibitor for its target protease (trypsin). Our studies have revealed that the inhibitor is extremely robust, which, coupled to its high potency of inhibition for KLK4 and concomitant blockade of PAR signaling, make it an excellent candidate for further therapeutic development.

EXPERIMENTAL PROCEDURES

Sparse Matrix Peptide Library Design and Peptide Synthesis

The sparse matrix library was based on Debela and Matsumura PS-SCL screens taking the top five scoring side chains at positions P1–P4, producing the matrix shown in Figure 1. Analysis of the interaction of SFTI with KLK4 showed that residues beyond Arg2 (P4 position on the inhibitor, subsite S4 on the enzyme) did not contact the enzyme and hence the library was restricted to tetrapeptides. Peptides were produced using standard solid phase synthesis protocols with 9-fluorenylmethyl carbamate (Fmoc) as semi-permanent protecting group. Peptide elongation was performed with 4 Eq. Fmoc amino acids dissolved in 0.25 M each of 2-(1H-benzotriazole-1-yl)-1, 1,3,3-tetramethyluronium hexafluorophosphate, 1-hydroxybenzotriazole, and N,N-di-isopropylethylamine (DIPEA) in N,N-dimethylformamide (DMF). Fmoc deprotection was achieved using 20% piperidine and 5% 1,8-diazabicyclo [5.4.0]undec-7-ene DBU in DMF.

Peptide-*p*NAs were synthesized as previously described (Abbenante et al., 2000), whereas peptide aldehydes were synthesized as above using H-Arg (Boc)-H Novasyn TG resin (Novabiochem). After removal of protecting groups with 95% trifluoroacetic acid with scavengers, cleavage was performed using 3 × 15 ml acetic acid/H_2O/dichloromethane/methanol (10:5:63:21) over 45 min.

SFTI was synthesized as a linear molecule on Fmoc-Asp(ODmab)-OH (Bachem) derivatized (0.5 mmol/g) 2-chloro trityl resin (Auspep). Using Fmoc-Cys(STBU)-OH (Bachem) enabled selective removal of the cysteine side chain protecting group (20 Eq dithiothreitol and 0.5 M DIPEA in DMF) before disulfide bond formation by overnight stirring in 10 mM reduced glutathione and 1 mM oxidized glutathione in Tris HCl (pH 8.0). Subsequent selective deprotection of the aspartate side chain Dmab-protecting group (five washes of two volumes 2% hydrazine in DMF enabled on resin cyclization through the aspartate side chain using 4 Eq each of DIPEA and 1-[Bis(dimethylamino)-methylene]-1H-1,2,3-triazolo[4,5-b]pyridinium 3-oxide hexafluorophosphate in DMF. Protecting group removal and cleavage was performed using 95% trifluoroacetic acid with scavengers. Lyophilized synthesis products were purified by reverse-phase HPLC from 10% isopropanol, 0.1% TFA in water with a Spherex 5 micron C18 column (Phenomenex), eluting with a linear gradient of 100% isopropanol and 0.1% TFA over 70 min. Molecular masses were determined using Protein Chip Send Arrays (Bio-Rad; #C57-30081) with a Protein Chip SELDI-TOF-MS system (Bio-Rad) in accordance with the manufacturer's instructions (see Supplemental Data available online).

Protein Expression and Purification

Human recombinant KLK4 was expressed in *E. coli* using a previously described chimeric KLK4 plasmid construct where the native proregion was replaced with the proregion of PSA, enabling autoactivation (Takayama et al., 2001). Protein was expressed as inclusion bodies that were isolated and solubilized as described previously to yield 90% pure KLK4. Protein refolding was performed by dilution into 100 volumes of refolding buffer I (2 M urea, 0.1 M NaCl, 5 mM GSH, 0.5 mM GSSG, 10 mM benzamidine, 50 mM Tris HCl [pH 8.0], 2 mM $CaCl_2$) over 44 hr before further dilution into 3 volumes refolding buffer II (refolding buffer I with 0.5 M urea, 0.5 mM GSH, 0.05 mM GSSG, 2 mM $CaCl_2$) over another 24 hr. Dialysis was performed as previously described (Takayama et al., 2001), with an additional 2 mM $CaCl_2$ added to reduce aggregation (Debela et al., 2006) before concentration using UNO sphere Q (Bio-Rad) and eluting with Tris-buffered saline (pH 7.5)/2 mM $CaCl_2$. Subsequently, the material was purified to apparent homogeneity (according to Coomassie-blue-stained SDS-PAGE) by gel filtration using Sephacryl S-200 (GE Health Care) pre-equilibrated with 50 mM Tris-HCl (pH 7.5), 20 mM NaCl, and 2 mM $CaCl_2$.

Insect cell kallikrein expression constructs for KLK2, 5, and 14 were generated by ligating kallikrein open reading frames, including the pre/proregion into the pIB/V5-His vector (Invitrogen); resulting constructs were validated by DNA sequencing. These constructs generate the complete kallikrein amino acid sequence followed by V5 (GKPIPNPLLGLDST) and 6x histidine tags. Insect Sf9 cells were transfected using Cellfectin (Invitrogen) as described previously (Ramsay et al., 2008b). Following transfection with the kallikrein-pIB/V5-His constructs, Sf9 cells with stably integrated kallikrein-pIB constructs were selected with 50 μg/ml Blasticidin (InvivoGen, San Diego, CA). Kallikreins were purified from conditioned media from these cells using Ni-NTA agarose as described by Ramsay et al. (2008a). Eluted fractions containing kallikreins, identified by analysis of a Coomassie-stained polyacrylamide gel, were pooled and then dialyzed against phosphate-buffered saline (PBS, pH 7.4) at 4°C overnight. Kallikreins were aliquoted and stored at −80°C. Recombinant protein was also validated by immunoblotting using anti-V5-His antibodies to confirm the identity of purified proteins (see Supplemental Data).

Chromogenic Substrate Screen

Peptide substrates were adjusted to equimolarity according to their absorbance at 405nm following total hydrolysis of the *p*NA moiety. Assays were performed in transparent 96 microwell plates with 4.9 ng KLK4 and 12 μM substrate in 300 μl assay buffer (0.1 M Tris HCl [pH 7.5], 0.1 M NaCl). Hydrolysis was monitored at 405 nm over 14 min using a Benchmark plus microspectrophotometer (Bio-Rad).

Kinetic Studies

Active site titration was carried out according to Beynon and Bond (1989), replacing α_1-proteinase inhibitor with soybean trypsin inhibitor. Enzymatic activity assays were performed with 4.9 nM KLK4, and substrate concentrations in the range of 0–600 μM in 300 μl assay buffer with hydrolysis monitored over 5 min as described for the substrate screen. The data were fitted to the Michaelis-Menten equation by linear regression analysis using the Prism 5 software suite (GraphPad Software Inc.).

Inhibitor Kinetics

Recombinant kallikreins were expressed in insect cells as described above or obtained from R&D Systems (Minneapolis, MN). All other enzymes and substrates were obtained from Sigma Chemicals if not otherwise specified. Insect cell KLK2 (150 ng), bacterially expressed human KLK4 (37 ng), insect cell KLK5 (60ng), insect KLK14 (70ng), bovine β-trypsin (20 ng), bovine thrombin (20 ng), bovine α-chymotrypsin (0.5 μg), *Streptomyces griseus* type XIV protease (0.5 μg), bovine plasminogen (0.5 μg), and human matriptase (30 ng, R&D Systems) were incubated with various concentrations of inhibitors in 200 μl assay buffer for 10 min prior to initiation by the addition of 100 μl of 0.3 mM peptide-pNA substrates Bz-PFR-*p*NA: KLK2; FVQR-*p*NA: KLK4; Bz-PFR-*p*NA: KLK5; Ac-GSLR-pNA: KLK14; BAPNA: trypsin; Bz-Phe-Val-Arg-*p*NA: thrombin and matriptase; Trp-*p*NA: α-chymotrypsin; Leu-*p*NA: *Streptomyces griseus* type XIV protease, and bovine plasma plasminogen. The release of *p*NA moiety was monitored as described above for 7 min, with each point being the average of three independent triplicate reactions. IC_{50} was determined using the Prism 5 software suite (GraphPad Software).

Stability of SFTI-FCQR in Cell-Based Systems

Cell monolayers of LNCaP, 22Rv1 and PC3 cells were established in RPMI 1640 medium supplemented with 10% fetal calf serum, 100 U/ml penicillin, and 100 μg/ml streptomycin. Each cell line was treated with ± 1 μM SFTI-FCQR contained in 4.0 ml RPMI media (as above) with a vehicle control to account for inhibition by intrinsic media factors. Samples (250 μl) of media were taken at 0, 24, 48, 72, 96, and 120 hr time points. Media samples were

boiled at 97°C for 15 min, and then centrifuged at 14,000 rpm for 5 min to remove cellular debris and precipitated protein. Residual SFTI-FCQR inhibitory activity in the medium was determined against recombinant KLK4 using FVQR-*p*NA as a peptide substrate as described above using 15 ng KLK4 and 0.1 mM FVQR-*p*NA with 2.5 μl and 50 μl media with or without SFTI-FCQR added from each treatment.

Protein Proteolysis

Fibrinogen was solubilized in assay buffer to a final concentration of 1 mg/ml and digested with proteases (with or without inhibitor) over varying periods at 37°C. Typically assays consisted of 5 μM protein substrate and 1–125 nM protease made up to a final volume of 8 μl with assay buffer. Proteolysis was initiated by addition of protease and terminated by addition of SDS-PAGE sample buffer and heat denaturation at 100°C for 5 min. Hydrolysis products were resolved on 12% SDS-PAGE gels and compared with incubations terminated immediately after initiation (time 0). The following incubation times and protease concentrations were used in this study: KLK2, 252 nM over 90 min; KLK4, 2.5 nM over 90 min, KLK5, 75 nM over 3 hr; KLK12 1.15 μM over 3 hr; KLK14, 125nM over 90 min; trypsin, 1 nM over 16 min.

Measurement of Changes in Intracellular Ca^{2+}

Lung murine fibroblasts from PAR-1-null mice stably expressing human PAR-2 were grown to 80% confluence as previously described (Ramsay et al., 2008b), washed with PBS, detached nonenzymatically, resuspended (4×10^6 cells/ml) in extracellular medium (121 mM NaCl, 5.4 mM KCl, 0.8 mM $MgCl_2$, 1.8 mM $CaCl_2$, 5.5 mM glucose, 25 mM HEPES [pH 7.4]) containing 0.2% (w/v) bovine serum albumin (Sigma), and then loaded with the fluorescence indicator Fura-2 acetoxymethyl ester (1.0 μM; Invitrogen) at room temperature for 60 min. Cells were then pelleted followed by resuspension in extracellular medium (without bovine serum albumin) at a concentration of 2×10^6 cells/ml for fluorescence measurements. The ratio of fluorescence at 510 nm after excitation at 340 and 380 nm was monitored (Polarstar Optima fluorescent plate reader) during treatment with bovine β trypsin (Sigma Chemicals), PAR-2-activating peptide SLIGKV (AusPep), and iKLK4 with or without 1 μM SFTI-FCQR.

Molecular Modeling

All modeling and superpositions were performed using COOT (Emsley and Cowtan, 2004). Residue packing and interatomic clashes were visualized and monitored in COOT using the programs REDUCE and PROBE (Davis et al., 2004). First, a KLK4-SFTI complex was modeled by superimposing KLK4 (Protein Data Bank [PDB] ID code 2BDG, chain A) with the trypsin chain of a trypsin-SFTI complex (PDB ID 1SFI) and removing any unfavorable interactions by conjugate gradient energy minimization with the program CNS (Brunger et al., 1998). Backbone atoms of both the protease and SFTI-FCQR molecule were fixed, in light of the rigidity of the inhibitor and structural conservation of KLK4 with trypsin, whereas side chains were subject to harmonic restraints. Molecular surfaces were created using CCP4MG (Potterton et al., 2004) and color coded according to electrostatic potential (calculated by the Poisson-Boltzmann solver within CCP4MG). The probe radius used was 1.4 Å. The resulting molecular surfaces were rendered using POVRAY (www.povray.org) (Figures 5 D and 5E). PyMol (http://pymol.sourceforge.net/newman/user/toc.html) was used to produce Figures 5A–5C.

SUPPLEMENTAL DATA

Supplemental Data include Supplemental Experimental Procedures and three figures and can be found with this article online at http://www.cell.com/chemistry-biology/supplemental/S1074-5521(09)00175-6.

ACKNOWLEDGMENTS

We thank Dan Abrahmsen for technical assistance, John Abbenante for guidance during *p*NA synthesis, and Elmar Kreiger and Zrinka Gattin for constructive criticism of SFTI molecular simulations. Funding was provided by the Cancer Council Queensland (grant 44323) and the Prostate Cancer Foundation of Australia (grant PR09).

Received: November 11, 2008
Revised: April 30, 2009
Accepted: May 8, 2009
Published: June 25, 2009

REFERENCES

Abbenante, J., Leung, D., Bond, T., and Fairlie, D.P. (2000). An efficient Fmoc strategy for the rapid synthesis of peptide para-nitroanilides. Lett. Pept. Sci. *7*, 347–351.

Arlt, M., Kopitz, C., Pennington, C., Watson, K.L.M., Krell, H.-W., Bode, W., Gansbacher, B., Khokha, R., Edwards, D.R., and Kruger, A. (2002). Increase in gelatinase-specificity of matrix metalloproteinase inhibitors correlates with antimetastatic efficacy in a T-cell lymphoma model. Cancer Res. *62*, 5543–5550.

Beaufort, N., Debela, M., Creutzburg, S., Kellermann, J., Bode, W., Schmitt, M., Pidard, D., and Magdolen, V. (2006). Interplay of human tissue kallikrein 4 (hK4) with the plasminogen activation system: hK4 regulates the structure and functions of the urokinase-type plasminogen activator receptor (uPAR). Biol. Chem. *387*, 217–222.

Beynon, R.J., and Bond, J.S. (1989). Proteolytic Enzymes: A Practical Approach (New York: Oxford University Press).

Brunger, A.T., Adams, P.D., Clore, G.M., DeLano, W.L., Gros, P., Grosse-Kunstleve, R.W., Jiang, J.S., Kuszewski, J., Nilges, M., Pannu, N.S., et al. (1998). Crystallography & NMR system: A new software suite for macromolecular structure determination. Acta Crystallogr. D Biol. Crystallogr. *54*, 905–921.

Chambers, A.F., and Matrisian, L.M. (1997). Changing views of the role of matrix metalloproteinases in metastasis. J. Natl. Cancer Inst. *89*, 1260–1270.

Coughlin, S.R. (1999). How the protease thrombin talks to cells. Proc. Natl. Acad. Sci. USA *96*, 11023–11027.

Coughlin, S.R. (2005). Protease-activated receptors in hemostasis, thrombosis and vascular biology. J. Thromb. Haemost. *3*, 1800–1814.

Daly, N.L., Chen, Y.-K., Foley, F.M., Bansal, P.S., Bharathi, R., Clark, R.J., Sommerhoff, C.P., and Craik, D.J. (2006). The absolute structural requirement for a proline in the P3′-position of Bowman-Birk protease inhibitors is surmounted in the minimized SFTI-1 scaffold. J. Biol. Chem. *281*, 23668–23675.

Darmoul, D., Marie, J.C., Devaud, H., Gratio, V., and Laburthe, M. (2001). Initiation of human colon cancer cell proliferation by trypsin acting at protease-activated receptor-2. Br. J. Cancer *85*, 772–779.

Davis, I.W., Murray, L.W., Richardson, J.S., and Richardson, D.C. (2004). MOLPROBITY: structure validation and all-atom contact analysis for nucleic acids and their complexes. Nucleic Acids Res. *32*, W615–W619.

Debela, M., Magdolen, V., Schechter, N., Valachova, M., Lottspeich, F., Craik, C.S., Choe, Y., Bode, W., and Goettig, P. (2006). Specificity profiling of seven human tissue kallikreins reveals individual subsite preferences. J. Biol. Chem. *281*, 25678–25688.

Descours, A., Moehle, K., Renard, A., and Robinson, J.A. (2002). A new family of beta-hairpin mimetics based on a trypsin inhibitor from sunflower seeds. ChemBioChem *3*, 318–323.

Emsley, P., and Cowtan, K. (2004). Coot: model-building tools for molecular graphics. Acta Crystallogr. D Biol. Crystallogr. *60*, 2126–2132.

Even-Ram, S., Uziely, B., Cohen, P., Grisaru-Granovsky, S., Maoz, M., Ginzburg, Y., Reich, R., Vlodavsky, I., and Bar-Shavit, R. (1998). Thrombin receptor overexpression in malignant and physiological invasion processes. Nat. Med. *4*, 909–914.

Gao, J., Collard, R.L., Bui, L., Herington, A.C., Nicol, D.L., and Clements, J.A. (2007). Kallikrein 4 is a potential mediator of cellular interactions between cancer cells and osteoblasts in metastatic prostate cancer. Prostate *67*, 348–360.

Henrikson, K.P., Salazar, S.L., Fenton, J.W., and Pentecost, B.T. (1999). Role of thrombin receptor in breast cancer invasiveness. Br. J. Cancer *79*, 401–406.

Hidalgo, M., and Eckhardt, S.G. (2001). Development of matrix metalloproteinase inhibitors in cancer therapy. J. Natl. Cancer Inst. *93*, 178–193.

Hilpert, K., Hansen, G., Wessner, H., Volkmer-Engert, R., and Hohne, W. (2005). Complete substitutional analysis of a sunflower trypsin inhibitor with different serine proteases. J. Biochem. *138*, 383–390.

Hollenberg, M.D. (2003). Proteinase-mediated signaling: Proteinase-activated receptors (PARs) and much more. Life Sci. *74*, 237–246.

Huck, C.W., Pezzei, V., Schmitz, T., Bonn, G.K., and Bernkop-Schnürch, A. (2006). Oral peptide delivery: Are there remarkable effects on drugs through sulfhydryl conjugation? J. Drug Target. *14*, 117–125.

Jemal, A., Siegel, R., Ward, E., Hao, Y., Xu, J., Murray, T., and Thun, M.J. (2008). Cancer Statistics, 2008. CA Cancer J. Clin. *58*, 71–96.

Korsinczky, M.L., Schirra, H.J., Rosengren, K.J., West, J., Condie, B.A., Otvos, L., Anderson, M.A., and Craik, D.J. (2001). Solution structures by 1H NMR of the novel cyclic trypsin inhibitor SFTI-1 from sunflower seeds and an acyclic permutant. J. Mol. Biol. *311*, 579–591.

Kruger, A., Soeltl, R., Sopov, I., Kopitz, C., Arlt, M., Magdolen, V., Harbeck, N., Gansbacher, B., and Schmitt, M. (2001). Hydroxamate-type matrix metalloproteinase inhibitor Batimastat promotes liver metastasis. Cancer Res. *61*, 1272–1275.

Li, P., Jiang, S., Lee, S.L., Lin, C.Y., Johnson, M.D., Dickson, R.B., Michejda, C.J., and Roller, P.P. (2007). Design and synthesis of novel and potent inhibitors of the type II transmembrane serine protease, matriptase, based upon the sunflower trypsin inhibitor-1. J. Med. Chem. *50*, 5976–5983.

Long, Y.Q., Lee, S.L., Lin, C.Y., Enyedy, I.J., Wang, S., Li, P., Dickson, R.B., and Roller, P.P. (2001). Synthesis and evaluation of the sunflower derived trypsin inhibitor as a potent inhibitor of the type II transmembrane serine protease, matriptase. Bioorg. Med. Chem. Lett. *11*, 2515–2519.

Luckett, S., Garcia, R.S., Barker, J.J., Konarev, A.V., Shewry, P.R., Clarke, A.R., and Brady, R.L. (1999). High-resolution structure of a potent, cyclic proteinase inhibitor from sunflower seeds. J. Mol. Biol. *290*, 525–533.

Malone, S., Perry, G., Segal, R., Dahrouge, S., and Crook, J. (2005). Long-term side-effects of intermittent androgen suppression therapy in prostate cancer: results of a phase II study. BJU Int. *96*, 514–520.

Matsumura, M., Bhatt, A.S., Andress, D., Clegg, N., Takayama, T.K., Craik, C.S., and Nelson, P.S. (2005). Substrates of the prostate-specific serine protease prostase/KLK4 defined by positional-scanning peptide libraries. Prostate *62*, 1–13.

Mize, G.J., Wang, W., and Takayama, T.K. (2008). Prostate-specific kallikrein-2 and −4 enhance the proliferation of DU145 prostate cancer cells through protease-activated receptors-1 and −2. Mol. Cancer Res. *6*, 1043–1051.

Nierodzik, M.L., Chen, K., Takeshita, K., Li, J.J., Huang, Y.Q., Feng, X.S., D'Andrea, M.R., Andrade-Gordon, P., and Karpatkin, S. (1998). Protease-activated receptor 1 (PAR-1) is required and rate-limiting for thrombin-enhanced experimental pulmonary metastasis. Blood *92*, 3694–3700.

Obiezu, C.V., Michael, I.P., Levesque, M.A., and Diamandis, E.P. (2006). Human kallikrein 4: enzymatic activity, inhibition, and degradation of extracellular matrix proteins. Biol. Chem. *387*, 749–759.

Overall, C.M., and Lopez-Otin, C. (2002). Strategies for MMP inhibition in cancer: innovations for the post-trial era. Nat. Rev. Cancer *2*, 657–672.

Potterton, L., McNicholas, S., Krissinel, E., Gruber, J., Cowtan, K., Emsley, P., Murshudov, G.N., Cohen, S., Perrakis, A., and Noble, M. (2004). Developments in the CCP4 molecular-graphics project. Acta Crystallogr. D Biol. Crystallogr. *60*, 2288–2294.

Ramsay, A.J., Dong, Y., Hunt, M.L., Linn, M., Samaratunga, H., Clements, J.A., and Hooper, J.D. (2008a). Kallikrein-related peptidase 4 (KLK4) initiates intracellular signaling via protease-activated receptors (PARs): KLK4 and PAR-2 are co-expressed during prostate cancer progression. J. Biol. Chem. *283*, 12293–12304.

Ramsay, A.J., Reid, J.C., Adams, M.N., Samaratunga, H., Dong, Y., Clements, J.A., and Hooper, J.D. (2008b). Prostatic trypsin-like kallikrein-related peptidases (KLKs) and other prostate-expressed tryptic proteinases as regulators of signalling via proteinase-activated receptors (PARs). Biol. Chem. *389*, 653–668.

Snyder, G.H., Cennerazzo, M.J., Karalis, A.J., and Locey, D. (1981). Electrostatic influence of local cysteine environments on disulfide exchange kinetics. Biochemistry *20*, 6509–6519.

Takayama, T.K., Fujikawa, K., and Davie, E.W. (1997). Characterization of the precursor of prostate-specific antigen. J. Biol. Chem. *272*, 21582–21588.

Takayama, T.K., McMullen, B.A., Nelson, P.S., Matsumura, M., and Fujikawa, K. (2001). Characterization of hK4 (prostase), a prostate-specific serine protease: activation of the precursor of prostate specific antigen (pro-PSA) and single-chain urokinase-type plasminogen activator and degradation of prostatic acid phosphatase. Biochemistry *40*, 15341–15348.

Veveris-Lowe, T.L., Lawrence, M.G., Collard, R.L., Bui, L., Herington, A.C., Nicol, D.L., and Clements, J.A. (2005). Kallikrein 4 (hK4) and prostate-specific antigen (PSA) are associated with the loss of E-cadherin and an epithelial-mesenchymal transition (EMT)-like effect in prostate cancer cells. Endocr. Relat. Cancer *12*, 631–643.

Xi, Z., Klokk, T.I., Korkmaz, K., Kurys, P., Elbi, C., Risberg, B., Danielsen, H., Loda, M., and Saatcioglu, F. (2004). Kallikrein 4 is a predominantly nuclear protein and is overexpressed in prostate cancer. Cancer Res. *64*, 2365–2370.

Zablotna, E., Jaskiewicz, A., Legowska, A., Miecznikowska, H., Lesner, A., and Rolka, K. (2007). Design of serine proteinase inhibitors by combinatorial chemistry using trypsin inhibitor SFTI-1 as a starting structure. J. Pept. Sci. *13*, 749–755.